IIETA International Information and Engineering Technology Association
Advancing the World of Information and Engineering

Journal of New Materials for Electrochemical Systems
Vol. 25, No.3, July 2022, pp.206-213
Journal homepage: http://iieta.org/journals/jnmes

Carboxymethyl Tamarind Kernel Gum /ZnO- Biocomposite: As an Antifungal and Hazardous Metal Removal Agent

Jagram Meena[ab], Harish Chandra[b], Sudhir G. Warkar* [a]

[a] Delhi Technological University, Delhi India 110042
[b] Gurukul Kangri (Deemed to be University) Haridwar-249404, Uttarakhand, India-249404

*Author for correspondence: sudhirwarkar@gmail.com

https://doi.org/10.14447/jnmes.v25i3.a08

Received: May 25-2022
Accepted: July 22-2022

Keywords:
Carboxymethyl tamarind kernel gum, zinc oxide NPs, antifungal, adsorption, chromium etc

ABSTRACT

ZnO nanoparticles (ZnO NPs) were in situ mixed with carboxymethyl tamarind kernel gum to generate the new biocomposite. High-resolution transmission electron microscopy (HR-TEM), field emission scanning electron microscopy (FE-SEM), Fourier transform infrared (FTIR), x-ray diffraction analysis (XRD), and dynamic light scattering (DLS)were used to characterize the CMTKG/ZnO nanocomposites. Numerous characterizations were utilized to prove that ZnO NPs had been integrated into the biopolymer matrix. The standard size of the CMTKG/ZnO nanocomposites was developed to be greater than 32–40 nm using high-resolution transmission electron microscopy and x-ray analysis de-Scherer methods. Chromium (VI) was removed from the aqueous solution using the nanocomposite (CMTKG/ZnO) as an adsorbent. The nanocomposite reached its maximum adsorption during 80 minutes of contact time, 30 mg/L chromium (VI) concentration, 2.0 g/L adsorbent part, and 7.0 pH. Further research into the antifungal activity of CMTKG/ZnO nanocomposites against *Aspergillus flavus* MTCC-2799 was conducted.

1. INTRODUCTION

In recent years, aquatic contamination has gained international attention as a deliberate environmental concern, particularly for a number of pollutants that are entering aquatic systems as a result of the unplanned rapid rise in the world's population, industrialization, urbanization, and the excessive use of agricultural fertilizers and chemical hazards [1]. Chromium is a substance that is used in paints and the chemical industry that poses a serious risk to the atmosphere [2]. It results in water supply contamination. Chromium exists in two oxidation states in hydrated situations: one is trivalent Chromium (III) and the other is hexavalent Chromium (VI) [3]. Due to the fact that ionic compounds containing Chromium (VI), like CrO_4^{2-} and H_2CrO_4, are more transportable and soluble than Cr (III). While chromium (III)-containing phases form a feeble cell barrier, chromium (VI)-containing phases more easily penetrate through cell membranes [4-5]. In fluid conditions, Cr (VI) is thought to be 100 times more dangerous than Cr (III) [6-7]. Cr (VI) has significantly higher mobility in water and so it can be converted into a variety of reactive and hazardous intermediates, eventually compromising human health due to its accumulating properties *[8-9].*

Chromium can be taken out of contaminated water through co-precipitation, chemical reduction, coagulation, ion exchange, and adsorption methods. Most of these techniques are often expensive. On the other hand, adsorption techniques are a good choice because they are safe for the environment, effective, and non-toxic. [10]. ZnO NPs showed distinctive chemical and physical characteristics. [11]. Due to their novel uses in adsorptions [12], sensor activity [13], heat treatment [14], antimicrobial activity [15], antifungal activity [16], wound healing [17], ultra-violet filtering [18], and excessive catalytic and photochemical activity [19–20], ZnO NPs have attracted the attention of researchers. Nearly all researchers concur that it's critical to create green nanomaterial in an aqueous medium. This is due to the fact that it is simple to conduct and has no effect on the environment.

Natural, non-toxic, renewable, and sustainable polymer alternatives include biopolymers. They are extensively employed in industry, medicine, agriculture, and the environment. Some of the biopolymers that find use in the biomedical and pharmaceutical sectors include chitin, chitosan, cellulose, tamarind, starch, and pectin [21]. Biopolymers such as alginate, chitosan, and starch provide excellent alternatives for matrix polymers because they contain a high concentration of hydroxyl groups in their chains, which offer a favorable environment for the formation of nanoparticles. [22] Biopolymers have also been demonstrated to be bio and mucoadhesive, biocompatible, biodegradable and non-aggravating hence explored in biomedical applications such as drug delivery, bio nanoreactors, nanofiltration, biosensors, and antibacterial activity. In two other studies [26, 27], polysaccharides extracted from Tamarindus indica seeds were modified to carboxymethyl tamarind seed kernel polysaccharide (CMTSP) and then used for drug delivery [26] and as enzyme [27].

In this study, precursor ZnO nanoparticles are combined with a matrix of carboxymethyl tamarind kernel gum to generate a CMTKG/ZnO biocomposite. The synthesized biocomposite showed remarkable stability, maximal accessibility, and intriguing enhancement brought on by nanoparticle-matrix interaction. The proposed study aimed to evaluate the performance of novel synthesized CMTKG/ZnO nanocomposite as an adsorbent for the removal of Chromium (VI) and also as an antifungal agent.

2. EXPERIMENTAL

2.1 Chemicals and reagents

Carboxymethyl tamarind kernel powder gum (CMTKG) (Courtesy Hindustan Gums Limited, India), Zinc acetate (CDH), Potassium dichromate (CDH), Acetone (CDH), Absolute alcohol (CDH), and double distilled water.

2.2. Synthesis of Cr (VI) solution

The solutions of Chromium (VI) (100 mg L^{-1}) used were prepared by dissolving $K_2Cr_2O_7$ in de-ionized water, which was weakened to desired focuses (10 - 80 mg/L).

2.3. Synthesis of nanocomposites

ZnO NPs were synthesized by the co-precipitation method. 0.05M zinc acetate solution was treated with 10 mL 0.05M alcoholic NaOH solution to reduce zinc acetate to ZnO NPs. At 60°C, this solution was continuously magnetically agitated to achieve homogeneity. To this solution, 1 g carboxymethyl tamarind kernel gum uniformly dispersed in 150 mL double distilled water was added and the mixing proceeded till a homogeneous solution was gotten for 24 hr. The final product obtained was immobilized ZnO NPs within the polymeric CMTKG (i.e. CMTKG/ZnO nanocomposite) precipitate. To get rid of any loose debased particles, the precipitate was sonicated at 10,000 rpm for 20 min. It was then washed with acetone. To obtain a dry powder of CMTKG/ZnO nanocomposite, the precipitate was then dried at 50 °C in the hot air oven after being washed with ethanol.

2.4 Characterization

2.4.1 Dynamic light scattering (DLS)

By analyzing the dynamic disparity in light scattering intensity caused by the Brownian velocity of the nanoparticles, the dynamic light scattering (DLS) Zetasizer was used to detect the size distribution of particles.

2.4.2 Fourier transform infrared (FTIR)

The Perkin Elmer FT-IR BX2 Instrument was used to study the infrared spectra (4000-400 cm^{-1}) for evaluations. The pellets were created by mixing 200 mg of KBr spectroscopic grade with 10 mg of the test sample.

2.4.3 Field Emission-Scanning electron microscopy (FE-SEM)

Scanning electron microscopy investigation of the surface morphology of CMTKG/ZnO nanocomposite was performed using Model: JEOL JSM-6610LV.

2.4.4 High-resolution transmission electron microscope (HR-TEM)

Using an ultrasonicator, 5 mg of dried CMTKG/ZnO nanocomposites were diluted in 25 mL of ethanol and subjected to a high-resolution transmission electron microscopy test. A 10 mL dispersion of nanocomposites was applied to a copper grid that was permanently coated.

2.4.5 X-ray diffraction (XRD)

X-ray diffraction studies of prepared CMTKG/ZnO nanocomposites were carried out using an X-ray diffractometer (P Analytical X'Pert Pro) at the current and voltage of 40 mA using Cu K α radiations (k = 1.5406 nm and λ=1.5406 Å) and scanning angle 2θ in the range of 0-80°.

2.5. Adsorption studies

Adsorption investigations were carried out using the batch method at room temperature. In a water-bath shaker, 10 mL of varied Chromium (VI) concentrations (ranging from 10 to 50 mg/L) were equilibrated with varying doses of CMTKG-ZnO nanocomposite (0.5 to 3.0 g/L) for durations of 10 to 100 minutes. The adsorbent was isolated from the solutions by centrifugation and the left-over convergence of chromium (VI) particles in the supernatant fluid. The left-over concentration of Cr (VI) in the filtrate was investigated by using a UV-Vis spectrophotometer. The adsorption tests were conducted with variable adsorbent doses and varying contact times at different concentrations of chromium (VI) for dynamic estimations. Additionally, the impact of changing pH from 2 to 10 on adsorption was investigated. Using diluted HCl or NaOH solutions (both 0.01 M), the various pH solutions were created. The average value is reported after each test was performed in triplicate. The amount of chromium (VI) absorbed per unit mass of adsorbent (qe, mg. g^{-1}) was then calculated using Equations 1 and 2.

$$q_e = (C_o - C_t) \times \frac{v}{w} \quad (1)$$

$$\%\, Adsoption = \frac{(C_o - C_t)}{C_o} \times 100 \quad (2)$$

Where, q_e is the equilibrium absorption capacity of chromium (VI) (mg g^{-1}), C_o is the initial concentration of chromium (VI) (mg L^{-1}), C_t is the concentration of chromium (VI) (mg L^{-1}) at time t, v is the volume of chromium (VI) utilized (L) and w is the weight of adsorbent (g) utilized.

2.6 Antifungal Activity

The antifungal efficacy of the synthesized nanocomposites was tested on *Aspergillus flavus* MTCC 2799. The standard culture of *Aspergillus flavus* MTCC 2799 was used to test the antifungal activity of a sample of CMTKG/ZnO nanocomposites using the poisoned food method [30]. Specifically, different concentrations of nanocomposites (1000 ppm, 2000 ppm, and 3000 ppm) were prepared by adding the appropriate amount into cooled molten Potato Dextrose Agar (PDA) media except the control plate (i.e. without nanocomposite), and after solidifying, 6 mm well was created accordingly with the help of sterile cork borer. Each well received 100 µl of spore suspension of *A. flavus* MTCC2799. Petri plates used for the test and control were incubated at 28 °C for 5 days while the fungus growth was continuously observed. Following incubation, the percentage of inhibition was estimated using the following formula:

$$\text{Inhibition of mycelial growth (\%)} = \frac{(Ac - At)}{Ac} \times 100 \quad (3)$$

where *Ac* is the mean diameter of the colony in the control sample, and *At* is the mean diameter of the colony in the treated sample. [30-31]

3. RESULTS AND DISCUSSION

3.1 Synthesis of CMTKG/ZnO nanocomposites

It is presumed that the ZnO NPs are attached to the CMTKG biopolymer matrix through H-bonding between the hydroxyl and ZnO NPs, as proposed in Scheme S_1.

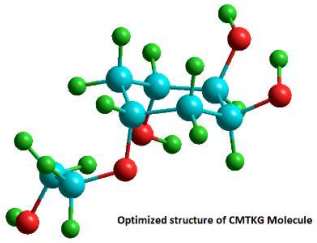

(a)

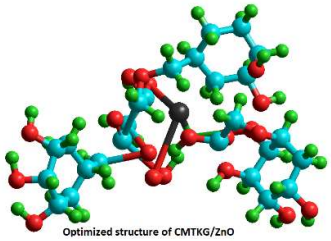

(b)

Scheme 1. Schematic presentations of Interaction of Solution with (a) CMTKG (b) CMTKG/ZnO biocomposite

3.1.1 Dynamic light scattering (DLS)

Using the Dynamics Light Scattering method, the particle size of manufactured ZnO NPs generated in-situ in CMTKG aqueous solution was measured. Figure 1 shows the size distributions of produced ZnO NPs. As can be observed, the majority of the particles have sizes between 56 and 76 nm, with 66 nm having the biggest size distributions. [32]

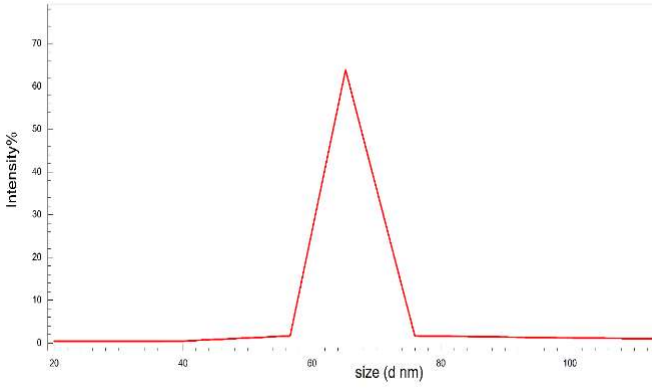

Figure 1. DLS analysis of CMTKG-ZnO NPs

3.1.2 Fourier transform infrared (FTIR)

FTIR spectra of CMTKG and CMTKG/ZnO composites are compared in Figure 2. Results showed that all characteristic peaks of CMTKG remained present in the CMTKG/ZnO nanocomposite, which indicates that the presence of ZnO NPs does not affect the chemical structure of CMTKG. However, peaks of 1110 and 1241 cm^{-1} indicate chemical interaction between CMTKG and ZnO NPs [25]

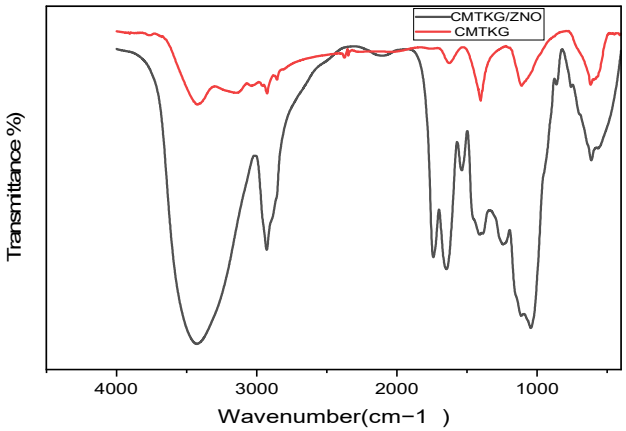

Figure 2. FTIR spectra of CMTKG & CMTKG/ZnO nano-composite

3.1.3 X-Ray diffractions (XRD)

Figure 3 illustrates the XRD spectra of CMTKG and CMTKG/ZnO nanocomposite. Results show that CMTKG crystal peaks are identical in both samples, which indicates that ZnO NPs do not interfere with the CMTKG. However, two distinct peaks of ZnO at 26° and 33° were found in the XRD spectra of the CMTKG/ZnO nanocomposite. Here, the crystal particle size was calculated by using Debye –Scherrer Equation as mentioned below

$$D = \frac{K\lambda}{\beta\cos\theta}$$

Here k=0.9, λ is the wavelength of source (1.5Å) β is the FWHM, and θ is the angle of diffraction. Based on XRD spectra, the average size of ZnO particles was found 31.69 nm. A similar observation was also reported in [32].

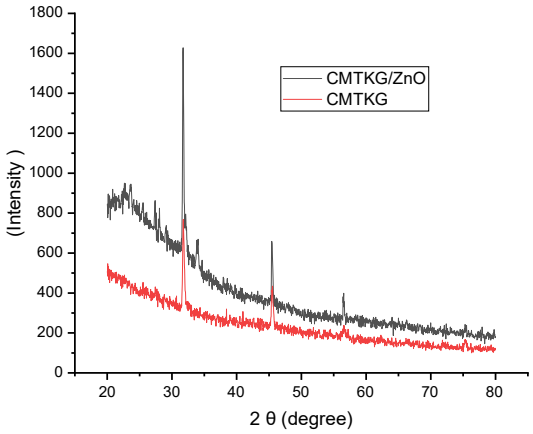

Figure 3. XRD spectra of CMTKG & CMTKG/ZnO nanocomposite

3.1.4 Field emission scanning electron microscopy (FE-SEM)

Scanning Electron Microscope (SEM) images of CMTKG and CMTKG/ZnO nanocomposite are shown in Figure 4. Figure 4 (a) shows the homogeneous morphology of the

CMTKG sample surface. ZnO particle shape and size are shown in Figure 4 (b). ZnO particles were rectangular in shape with an average cross-section area of 120 nm × 220 nm and 10 to 15 nm thickness. SEM image (Figure 4 (b)) also shows the intercalation and exploration of nanoparticle layers. A comparable finding was also reported in [33].

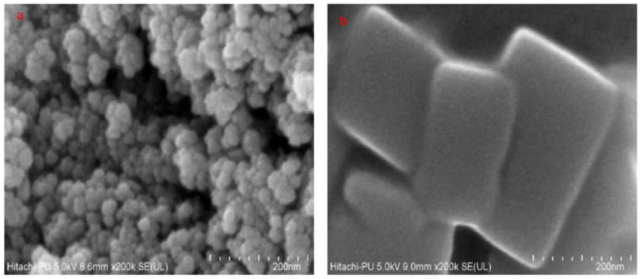

Figure 4. SEM images (a) CMTKG; (b) CMTKG/ZnO nano-composite

3.1.5 High resolution transmission electron microscope (HR-TEM)

The transmission electron microscopic (TEM) image of the CMTKG/ZnO nanocomposite is shown in Figure 5 (a). ZnO NPs are visible as dark spots in the TEM image. The image shows that the ZnO NPs are well dispersed throughout the polymeric matrix. The average particle size was found 40-90 nm in TEM study (Figure 5 (b). A similar observation was also reported in [35].

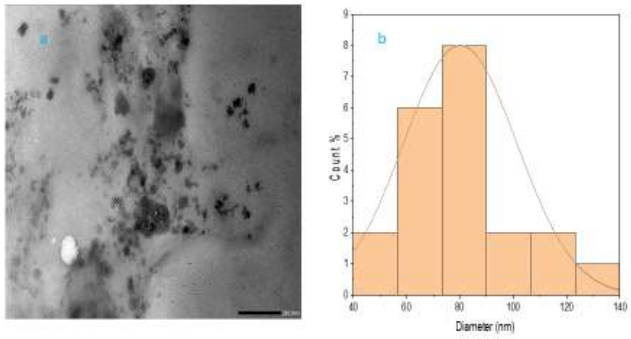

Figure 5. TEM Analysis (a) HR-TEM image of CMTKG/ZnO sample; (b) Particle size analysis

3.2. Adsorption Studies

3.2.1 Effects of Contact Time

The effects of contact time of Chromium (VI) extraction are reported in Figure 6 (a). These experiments were performed with the constant initial concentration of Chromium (VI) in feed (30 mg/L), and a constant amount of adsorbent CMTKG/ZnO nanocomposite (2 mg/L), with varying contact times of 10 minutes of 80 minutes. Performance of adsorbent is analyzed in terms of percent Chromium (VI) extraction and q_e as defined in Equations (1) and (2). Results show that values of percent extraction and q_e both increased with increasing contact time during adsorption experiments and reached a maximum value between 70 to 80 minutes, which is found as the optimum contact time to achieve maximum Chromium (VI) removal. The maximum percent extraction of Chromium (VI) was found at 95.5% in these experiments. The rapid rise in percent adsorption and adsorption efficiency at the beginning is due to the concentration gradient between Chromium in solution and in adsorbent and also attributed to the available vacant sites. [36]

3.2.2 Effects of adsorbent dose

Effects of adsorbent dose on chromium removal are shown in Figure 6 (b). These experiments were performed at a constant contact time of 80 minutes, at constant initial Chromium (VI) concentration in feed (30 mg/L), and with varying adsorbent amounts from 0.01 mg/L to 3.0 mg/L. Results showed that values of percent extraction of Chromium (VI) ions were increased with increasing adsorbent dose. However, values of q_e decreased with increasing adsorbent concentration. q_e is defined as the removal of Chromium (VI) ions per unit weight of adsorbent (Equation (2)). Thus, q_e represents the efficiency of the adsorbent in a particular experiment. Therefore, these results indicate that although the percent removal of chromium increases with increasing adsorbent concentration but the efficiency of adsorbent decreases with increasing its concentration. The maximum percent extraction of Chromium (IV) (93.40%) was found with a 3 mg/L adsorbent concentration. Greater availability of adsorption sites and sorptive surface area may be the cause of the increase in the percentage of adsorbate ions removed with an increase in adsorbent dosage.[9]

3.2.3 Effects of initial Chromium (VI) concentration

Effects of initial Chromium (VI) concentration on percent extraction and q_e are shown in Figure 6 (c). These experiments were performed at constant contact time (80 minutes), at a constant adsorbent dose (2 mg/L), and with varying initial Chromium (VI) concentrations from 18 mg/L to 32 mg/L. Results show that q_e of Chromium was increased with increasing its initial concentration, which suggests that adsorbent particles were not saturated with chromium ions and more chromium can be removed with the same amount of adsorbent. On the other hand, values of percent extraction decreased with increasing initial Chromium (VI) concentration in the feed. Maximum percent extraction of Chromium (VI) (93%) was found at 18 mg/L initial Chromium (VI) concentration in the feed. This was expected given the initial Cr (VI) concentrations, which served as the primary impetus to overcome the barriers to the mass transfer of Cr (VI) between the bulk and reactive sites.[44]

3.2.4 Effects of feed pH

The effects of feed pH on the adsorption capability of adsorbent (CMTKG/ZnO nanocomposite) are shown in Figure 6 (d). These experiments were performed at constant contact time (80 minutes), constant adsorbent dose (2 mg/L), constant initial concentration of Chromium (VI) in feed (30 mg/L), and with varying feed pH from 2 to 10. Results show that both percent extraction of Chromium (VI) and adsorbent efficiency (q_e) both increase with increasing pH values in the acidic region, reached maximum values at neutral pH (7), and then reduced with increasing pH values in the basic region. These results confirm that the performance of synthesized CMTKG/ZnO nanocomposite adsorbent for Chromium (VI) extraction strongly depends on the feed pH, and maximum extraction is achieved at 7 pH. At lower pH conditions, less interaction of Cr (VI) with adsorbent was noted and the H^+ compete with Cr (VI) hence observing less adsorption. It has

been hypothesized that at low pH levels, species are primarily adsorbed in their molecular form, but at higher pH levels, species are primarily adsorbed in their ionized form [45]. These findings support the electrostatic attraction of the anionic Cr (VI) species since the Cr (VI) species that developed under these circumstances are most likely to be $HCrO_4^-$ and $Cr_2O_7^{2-}$ anions. However, if pH rises, the efficacy of Cr (VI) adsorption and removal decreased concurrently as the concentration of the hydroxyl (OH^-) ion rose and electrostatically competed with anionic Cr (VI) species.

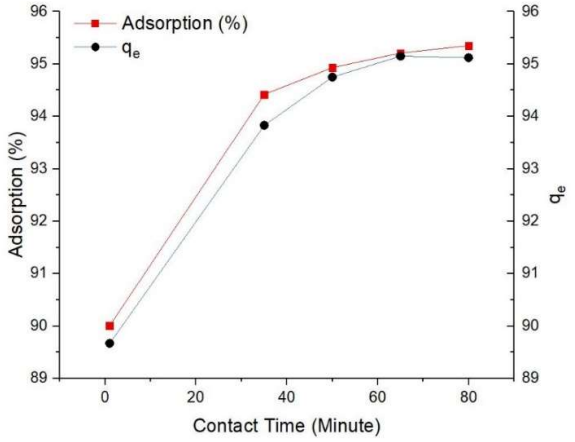

(a)

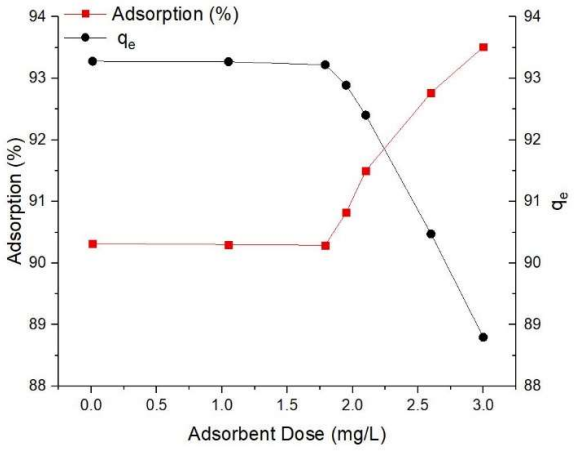

(b)

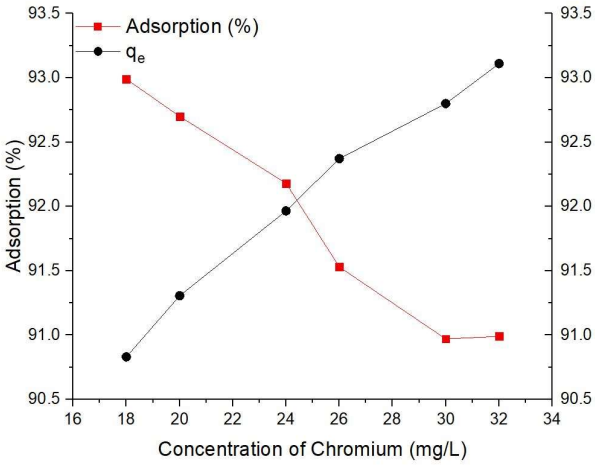

(c)

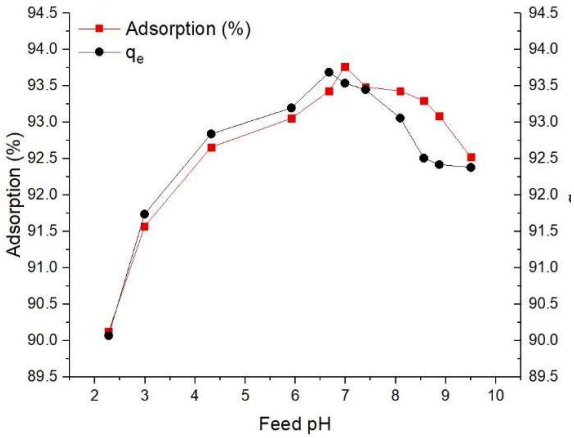

(d)

Figure 6. Adsorption of Chromium (VI) on CMTKG/ZnO nanocomposite: (a) Effects of contact time (b) Effects of adsorbent (CMTKG/ZnO nanocomposite) dose (c) Effects of initial Chromium concentrations in feed (d) Effects of feed pH

In Table 1, the performance of the synthesized adsorbent (CMTKG/ZnO nanocomposite) are compared with previously reported adsorbents. The performance of the CMTKG/ZnO adsorbent was found far better than the other traditional adsorbents reported in the literature for removal Chromium (VI) extraction, which depicts the novelty of the present study for the chromium removal from wastewater with prepared CMTKG/ZnO nanocomposites.

Table 1. Comparison studies of various bio-composite for removal of chromium (VI) ions

Adsorbent	Percent Extraction	Reference
CMTKG/ZnO	95.5	Present Study
GG/ZnO biocomposite	55.56	[11]
Activated carbon	3.46	[37]
PPy/GO	9.56	[38]
Activated carbon /magnetite	57.37	[39]
Mycelian/ carboxymethyl-cellulose	32.20	[40]
Poly-(methyl acrylate)guar gum	29.67	[41]

3.3. Antifungal Activities of CMTKG/ZnO nanocomposites.

Table 2 shows the antifungal activity of CMTKG/ZnO nanocomposites. The antifungal activity of CMTKG/ZnO nanocomposites was determined against *A. flavus* MTCC2799. The different concentration (in ppm) was evaluated against the radial growth of *A. flavus* MTCC 2799. The result shows the highest concentration i.e., 3000 ppm was the most effective concentration which inhibit the 50% radial growth of tested fungi followed by 2000 ppm (Figure7). However lower concentration i.e., 1000 ppm only inhibited 26.0 % of radial growth. As a result, CMTKG/ZnO nanocomposites were discovered to have natural antifungal

activity. The antifungal activity of Zinc oxide nanoparticle due to the production of Reactive Oxygen Species (ROS) which result in Oxidative stress [42-43]

Table 2. Percentage radial growth inhibition of *Aspergillus flavus* MTCC2799

Conc.	Growth area (mm)	Aver. Area Growth (in mm)	Inhibition (%)
Control	56.0,54.0 mm	55.0 ± 1.41mm	00.00%
1000ppm	40.0, 41.0mm	40.5 ± 0.70 mm	26.36%
2000ppm	34.0, 37.0mm	35.5 ± 2.12 mm	35.45%
3000ppm	27.0, 28.0 mm	27.5 ± 0.70 mm	50.00%

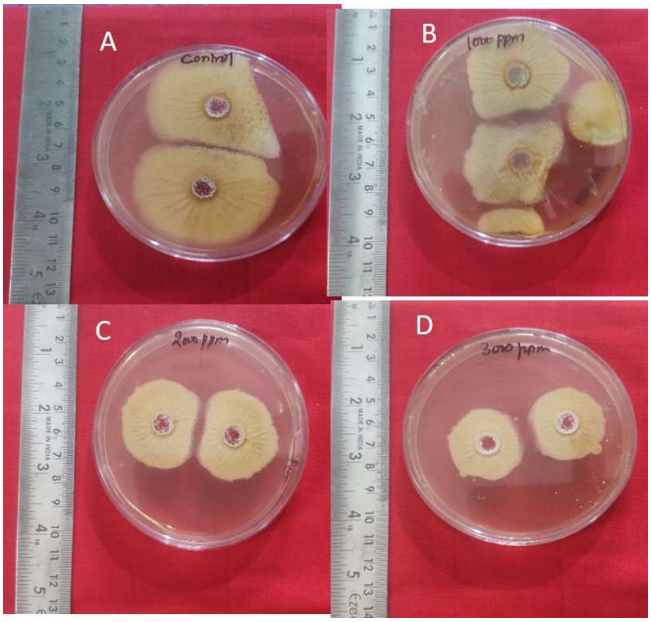

Figure 7. Percentage radial growth inhibition of CMTKG/ZnO nanocomposites *against Aspergillus flavus* MTCC-2799 at different concentrations (A) Control, (B) 1000 ppm, (C) 2000 ppm, and (D) 3000 ppm

4. CONCLUSION

In the present study, a novel CMTKG/ZnO nanocomposite was synthesized by using the in-situ method. FTIR and XRD characterizations indicated the presence of ZnO NPs which did not affect the chemical structure of CMTKG. However, chemical interaction between polymeric matrix and nanoparticle was found in FTIR spectra. SEM and TEM images confirm the homogeneous distribution of the ZnO NPs in a polymeric matrix with an average nanoparticle size of 40 to 90 nm. The prepared nanocomposite was then analyzed as an adsorbent for Chromium (VI) removal. Contact time 80 minutes, adsorbent loading 2 mg/L, initial Chromium (VI) concentration 30 mg/L and feed pH 7 was found as optimum operating parameters for maximizing percent extraction of Chromium (VI) ions (95.5%) from wastewater. The prepared composite was then examined as Antifungal material. *A. flavus* MTCC 2799 growth was successfully prepared by CMTKG/ZnO nano-composites.

ACKNOWLEDGMENTS

The authors would like to thank Delhi Technological University, Delhi, India, and Gurukul Kangri (Deemed to be University), Hardwar India for providing laboratory facilities. The authors would like to thank SAIF lab Chandigarh for providing the characterization facilities.
Conflicts of Interest- There is no conflict of interest among the author

REFERENCES

[1] Zhang, Lei, Yuexian Zeng, and Zhengjun Cheng. "Removal of heavy metal ions using chitosan and modified chitosan: A review." *Journal of Molecular Liquids* 214 (2016): 175-191.
[2] Gaballah, I., Kilbertus, G., 1998. Recovery of heavy metal ions through decontamination of synthetic solutions and industrial effluents using modified barks. J. Geochem. Explor. 62, 241–286.
[3] Fellenz, N. et al. Chromium (VI) removal from water by means of adsorption-reduction at the surface of amino-functionalized MCM-41 sorbents. Mesopor. Mater. 239, 138–146 (2017)
[4] Gokila, S.; Gomathi, T.; Sudha, P.N.; Anil, S. Removal of the heavy metal ion chromiuim(VI) using Chitosan and Alginate nanocomposites. Int. J. Biol. Macromol. 2017, 104, 1459–1468
[5] Zhitkovich, A. Chromium in drinking water: sources, metabolism, and cancer risks. Chem. Res. Toxicol. 24, 1617–1629 (2011).
[6] Megharaj, M., Avudainayagam, S. & Naidu, R. Toxicity of hexavalent chromium and its reduction by bacteria isolated from soil contaminated with tannery waste. Curr. Microbiol. 47, 51–54 (2003).
[7] Katz, S. A. Salem, H. Te Biological and Environmental Chemistry of chromium. (VI) CH Publishers, New York, 1994).
[8] Zheng, Zhihong and Xiaohan Duan. "Mitigating the Health Effects of Aqueous Cr (VI) with Iron-Modified Biochar." International Journal of Environmental Research and Public Health 19.3 (2022): 1481.
[9] Khan, Tabrez A., "Removal of chromium (VI) from aqueous solution using guar gum–nano zinc oxide biocomposite adsorbent." *Arabian Journal of Chemistry* 10 (2017): S2388-S2398.
[10] Warkar, S. G., Meena, J. (2022). Synthesis and applications of biopolymer /FeO nanocomposites: A review. Journal of New Materials for Electrochemical Systems, Vol. 25, No. 1, pp. 7-16.
[11] A. Barzinjy, Azeez. "Structure, Synthesis, and Applications of ZnO Nanoparticles: A Review." Jordan Journal of Physics 13.2 (2020): 123-135.
[12] K. Prasad and K. Anal Jha, "ZnO nanoparticles: synthesis and adsorption study," Natural Science, vol. 1, no. 2, pp. 129–135, 2009
[13] Ma, Q.; Lin, Z.-H.; Yang, N.; Li, Y.; Su, X.-G. A novel carboxymethyl chitosan–quantum dot-based intracellular probe for Zn2+ ion sensing in prostate cancer cells. Acta Biomater. 2014, 10, 868–874.
[14] Kumar, Pawan, et al. "The influence of post-growth heat treatment on the optical properties of pulsed laser deposited ZnO thin films." Applied Physics A 128.5 (2022): 1-9.

[15] U. Rajamanickam, P. Mylsamy, S. Viswanathan, and P. Muthusamy, "Biosynthesis of zinc nanoparticles using actinomycetes for antibacterial food packaging," in Proceedings of the International Conference on Nutrition and Food Sciences (IPCBEE '12), vol. 39, 2012.

[16] Akpomie, Kovo G., et al. "One-pot synthesis of zinc oxide nanoparticles via chemical precipitation for bromophenol blue adsorption and the antifungal activity against filamentous fungi." Scientific reports 11.1 (2021): 1-17.

[17] Hasanin, Mohamed, et al. "Novel design of bandages using cotton pads, doped with chitosan, glycogen and ZnO nanoparticles, having enhanced antimicrobial and wounds healing effects." International Journal of Biological Macromolecules 197 (2022): 121-130.

[18] Serpone, Nick, Daniele Dondi, and Angelo Albini. "Inorganic and organic UV filters: Their role and efficacy in sunscreens and suncare products." Inorganica chimica acta 360.3 (2007): 794-802

[19] Marci, Giuseppe, et al. "Preparation characterization and photocatalytic activity of polycrystalline ZnO/TiO2 systems. 2. surface, bulk characterization, and 4-nitrophenol photodegradation in liquid-solid regime." The Journal of Physical Chemistry B 105.5 (2001): 1033-1040.

[20] Singh, Simranjit, et al. "Citrulline rich structurally stable zinc oxide nanostructures for superior photocatalytic and optoelectronic applications: A green synthesis approach." Nano-Structures & Nano-Objects 11 (2017): 1-6.

[21] Verma, Devendra Kumar, et al. "Synthesis, characterization, and applications of chitosan-based metallic nanoparticles: A review." Journal of Applied and Natural Science 13.2 (2021): 544-551.

[22] Wang, Cong, et al. "Preparation, characterization and application of polysaccharide-based metallic nanoparticles: a review." Polymers 9.12 (2017): 689.

[23] J. Meena, polyaniline/carboxymethyl guar gum nanocomposites; as biodegradable conductive-film" Rasayan J. Chem., 15(2), 1021-1027 (2022) http://doi.org/10.31788/RJC.2022.1526820

[24]Bhat, Pratima, and P. Nagaraju. "Synthesis and characterization of ZnO-MWCNT nanocomposites for 1-butanol sensing application at room temperature." Physica B: Condensed Matter 570 (2019): 139-147

[25] Khushbu, Warkar Sudhir G., and Anil Kumar. "Synthesis and assessment of carboxymethyl tamarind kernel gum based novel superabsorbent hydrogels for agricultural applications." Polymer 182 (2019): 121823.

[26] Pandit, Ashlesha, Pravin, et al. "Carboxymethyl tamarind seed kernel polysaccharide formulated into pellets to target at colon." Indian J. Pharm. Educ. Res 52 (2018): 363-373

[27] Singh, Vandana, and Pramendra Kumar. "Carboxymethyl tamarind gum–silica nanohybrids for effective immobilization of amylase." Journal of Molecular Catalysis B: Enzymatic 70.1-2 (2011): 67-73.

[28] Goyal, Puja, Vineet Kumar, and Pradeep Sharma. "Carboxymethylation of tamarind kernel powder." Carbohydrate Polymers 69.2 (2007): 251-255.

[29] Da Silva, Bruna Lallo, et al. "Relationship between structure and antimicrobial activity of zinc oxide nanoparticles: An overview." International journal of nanomedicine 14 (2019): 9395.

[30] Adjou, E. S., S. Kouton, E. Dahouenon-Ahoussi, C. K. Sohounhloue, and M. M. Soumanou, "Antifungal activity of Ocimum canum essential oil against toxicogenic fungi isolated from peanut seeds in post-harvest in Benin," International Research Journal of Biological Sciences, vol. 1, no. 7, pp. 20–26, 2012.

[31] Chandra, H., Srivastava, J. K. and Agarwal, R. K. 2016. Fundamental Techniques in Microbiology. John Publisher Pvt. Ltd, New Delhi ISBN: 978-81-928544-1-0

[32] Singh, Simranjit, et al. "Citrulline rich structurally stable zinc oxide nanostructures for superior photo catalytic and optoelectronic applications: A green synthesis approach." Nano-Structures & Nano-Objects 11 (2017): 1-6.

[33] A. Barzinjy, Azeez. "Structure, Synthesis and Applications of ZnO Nanoparticles: A Review." Jordan Journal of Physics 13.2 (2020): 123-135.

[34] Jain, Devendra, et al. "Microbial fabrication of zinc oxide nanoparticles and evaluation of their antimicrobial and photocatalytic properties." Frontiers in chemistry 8 (2020): 778.

[35] Pal, Sagar, et al. "Carboxymethyl tamarind-g-poly (acrylamide)/silica: a high-performance hybrid nanocomposite for adsorption of methylene blue dye." Industrial & Engineering Chemistry Research 51.48 (2012): 15546-15556.

[36] Shen, Y.F., Tanga, J., Nie, Z.H., Wang, Y.D., Ren, Y., Zuo, L., 2009. Preparation and application of magnetic Fe3O4 nanoparticles for wastewater purification. Sep. Purif. Technol. 68, 312–319.

[37] Selvi, K., Pattabhi, S. and Kadirvelu, K. Removal of Cr (VI) from aqueous solution by adsorption onto activated carbon. *Bioresour. Technol.* 80, 87–89 (2001)

[38] Li, Shangkun, et al. "Fabrication of polypyrrole/graphene oxide composite nanosheets and their applications for Cr (VI) removal in aqueous solution." PLoS One 7.8 (2012): e43328.

[39] Nethaji, S., A. Sivasamy, and A. B. Mandal. "Preparation and characterization of corn cob activated carbon coated with nano-sized magnetite particles for the removal of Cr (VI)." *Bioresource Technology* 134 (2013): 94-100.S2388-S2398.

[40] Arıca, M.Y., Bayramoglu, G., 2005. Cr (VI) biosorption from aqueous solutions using free and immobilized biomass of Lentinus sajorcaju: preparation and kinetic characterization. Colloids Surf., A 253, 203–211

[41] Singh, V., et al. "Removal of cadmium from aqueous solutions by adsorption using poly (acrylamide) modified guar gum–silica nanocomposites." Separation and Purification Technology 67.3 (2009): 251-261

[42] Hirota, K.; Sugimoto, M.; Kato, M.; Tsukagoshi, K.; Tanigawa, T.; Sugimoto, H. Preparation of zinc oxide ceramics with a sustainable antibacterial activity under dark conditions. Ceram. Int. 2010, 36, 497−506.

[43] Xu, X.; Chen, D.; Yi, Z.; Jiang, M.; Wang, L.; Zhou, Z.; Fan, X.; Wang, Y.; Hui, D. Antimicrobial mechanism based on H2O2 generation at oxygen vacancies in ZnO crystals. Langmuir 2013, 29, 5573−5580

[44] Luo, Peng, et al. "Preparation and characterization of silane coupling agent modified halloysite for Cr (VI)

removal." Industrial & engineering chemistry research 50.17 (2011): 10246-10252.

[45] Bhattacharyya, Krishna G., and Susmita Sen Gupta. "Adsorption of chromium (VI) from water by clays." *Industrial & Engineering Chemistry research* 45.21 (2006): 7232-7240.